Modulating Photoluminescence of Monolayer Molybdenum Disulfide by Metal–Insulator Phase Transition in Active Substrates

Jiwei Hou, Xi Wang, Deyi Fu, Changhyun Ko, Yabin Chen, Yufei Sun, Sangwook Lee, Kevin X. Wang, Kaichen Dong, Yinghui Sun, Sefaattin Tongay, Liying Jiao, Jie Yao, Kai Liu,* and Junqiao Wu*

The atomic thickness and flatness allow properties of 2D semiconductors to be modulated with influence from the substrate. Reversible modulation of these properties requires an "active," reconfigurable substrate, i.e., a substrate with switchable functionalities that interacts strongly with the 2D overlayer. In this work, the photoluminescence (PL) of monolayer molybdenum disulfide (MoS_2) is modulated by interfacing it with a phase transition material, vanadium dioxide (VO_2). The MoS_2 PL intensity is enhanced by a factor of up to three when the underlying VO_2 undergoes the thermally driven phase transition from the insulating to metallic phase. A nonvolatile, reversible way to rewrite the PL pattern is also demonstrated. The enhancement effect is attributed to constructive optical interference when the VO_2 turns metallic. This modulation method requires no chemical or mechanical processes, potentially finding applications in new switches and sensors.

Dr. J. Hou, Y. F. Sun, Prof. K. Liu
State Key Laboratory of New Ceramics and Fine Processing
School of Materials Science and Engineering
Tsinghua University
Beijing 100084, P. R. China
E-mail: liuk@tsinghua.edu.cn

Dr. X. Wang, Dr. D. Fu, Dr. C. Ko, Dr. Y. Chen, K. X. Wang,
K. Dong, Prof. J. Yao, Prof. J. Wu
Department of Materials Science and Engineering
University of California
Berkeley, CA 94720, USA
E-mail: wuj@berkeley.edu

Prof. S. Lee
School of Materials Science and Engineering
Kyungpook National University
Daegu 41566, Korea

K. Dong
Department of Precision Instrument
Tsinghua University
Beijing 100084, P. R. China

Prof. Y. H. Sun
Department of Physics
School of Mathematics and Physics
University of Science and Technology Beijing
Beijing 100083, P. R. China

Prof. S. Tongay
School for Engineering of Matter
Transport and Energy
Arizona State University
Tempe, AZ 85287, USA

Prof. L. Jiao
Key Laboratory of Organic Optoelectronics and Molecular Engineering
of the Ministry of Education
Department of Chemistry
Tsinghua University
Beijing 100084, P. R. China

Prof. J. Yao, Prof. J. Wu
Materials Sciences Division
Lawrence Berkeley National Laboratory
Berkeley, CA 94720, USA

1. Introduction

2D transition metal dichalcogenides (TMDs) attract strong research attention due to their diverse physical properties and potential for device applications.[1,2] Monolayer semiconducting TMDs, such as MoS_2 and WS_2, have direct band gaps in contrast to indirect band gaps in their bulk counterparts.[3,4] Their photoluminescence (PL) efficiency is thus dramatically enhanced at the monolayer limit, potentially inspiring optoelectronic applications.[5–9] On the other hand, modulation of properties of 2D semiconductors is of vital importance for their ultimate applications. Electrostatic gating,[10,11] chemical doping,[12–14] strain,[15,16] etc., have been utilized to modulate both optical emission and electrical conductivity of 2D TMDs. These methods require either microfabrication or processing steps, or significant modification of the surface chemistry of 2D semiconductors. It is desired to develop a more convenient means to reversibly modulate their physical properties.

It has been reported that the PL peak position and intensity of a monolayer TMD are strongly dependent on the substrate where it sits. The mechanism behind this, however, is rather complicated. In 2D semiconductors such as MoS_2 monolayers, recombination of excitons (electron–hole pairs) or trions (electron–electron–hole clusters), depending on the background-free electron density, dominates the PL spectrum.[10,17] Charge transfer between the monolayer and substrate can alter the free carrier density of the monolayer and the spectral weights of excitons and trions.[18–20] Dielectric screening of Coulomb potentials is also found to affect the binding energies of excitons and trions, hence their PL intensities.[21] Strain, which may be imposed to the monolayer by the substrate or during the transfer process, is another factor in affecting the PL of the monolayer.[22] Lastly, light interference resulting from reflection and refraction also influences local electric fields (E-fields) around the monolayer, leading to strengthened or weakened absorption in and emission from the monolayer.[18,23,24] This wide variety of mechanisms offer ways to modulate the PL of 2D TMD monolayers by using an "active" substrate to modify the dielectric, electronic, and optical environments of the monolayers.

In this work, we utilize a phase transition material, vanadium dioxide (VO_2), to modulate the PL intensity of monolayer MoS_2. Changes in dielectric properties of VO_2 across the metal–insulator transition (MIT) alter the interference of light in the MoS_2 layer in such a way that the detected MoS_2 PL intensity is greatly enhanced when the VO_2 switches to the metallic phase from the insulating phase. The existence of similar PL enhancement with an insertion of insulating boron nitride (h-BN) layers between MoS_2 and VO_2, as well as the almost unchanged spectral weight ratios of trions to excitons of MoS_2 across the MIT of VO_2, excludes strain, charge transfer, or dielectric screening effects as the dominant mechanism. A nonvolatile, reversible method to rewrite the PL pattern is also demonstrated. This modulation is reversible and does not involve chemical or mechanical processes, and can be generalized to other 2D layers, potentially finding applications in switches and sensors based on 2D semiconductors.

2. Results

Monolayer MoS_2 samples were synthesized by chemical-vapor deposition (CVD) and then transferred onto a SiO_2/Si substrate (**Figure 1**a) or a VO_2 thin film (thereafter denoted as MoS_2/VO_2, Figure 1b). The details of fabrication are described in Experimental Section. VO_2 is a strongly correlated electronic material. It undergoes a thermally driven MIT at 68 °C accompanied with a structural phase transition from monoclinic in the low-temperature (insulating) phase to rutile in the high-temperature (metallic) phase.[25] VO_2 does not have PL emission in the spectral range near the PL wavelength of MoS_2 (Figure 1c). The PL of monolayer MoS_2 on a SiO_2/Si substrate ($MoS_2/SiO_2/Si$) consists of two closely spaced peaks. They are attributed to the A and B excitons in MoS_2, respectively, centered at around 1.9 eV and 2.0 eV (Figure 1c), which results from optical transitions from the conduction band to the two spin-orbital split valence bands.[3,4]

Raman spectra of the MoS_2/VO_2 clearly show a combined feature of MoS_2/SiO_2 and VO_2 (Figure 1d). The VO_2 monoclinic phase has vibration modes including A_g and B_g modes at 196 cm⁻¹, 225 cm⁻¹, 261 cm⁻¹, 309 cm⁻¹, 390 cm⁻¹, and 620 cm⁻¹.[26,27] In contrast, in this measurement configuration, MoS_2 exhibits only the in-plane mode (E_{2g}^1) and the out-of-plane mode (A_{1g}) at 387 cm⁻¹ and 406 cm⁻¹, respectively, on SiO_2.[28,29] The separation of 19 cm⁻¹ between the E_{2g}^1 and A_{1g} peaks confirms that the MoS_2 is monolayer.[28] When placed on VO_2, the A_{1g} mode of MoS_2 does not change, while the E_{2g}^1 mode red-shifts by ≈2 to 385 cm⁻¹ (Figure S1, Supporting Information). It is known that the A_{1g} mode is related to the doping level[30,31] and the E_{2g}^1 mode is sensitive to strain in MoS_2.[32] Therefore the unchanged A_{1g} mode and the shifted E_{2g}^1 mode of MoS_2 imply that the strain relaxes differently for MoS_2/VO_2 compared to MoS_2/SiO_2, which may result from the additional strain on MoS_2 imposed by the relatively rough VO_2 surface (Figure S2, Supporting Information) during the wet transfer process.

As VO_2 undergoes the transition from the insulating to metallic phase with increasing temperature, most of its physical properties change abruptly and drastically, including optical reflection and absorption, lattice symmetry and constants, conductivity and electron density, as well as band structure and work function.[33–35] Along with these changes, the color of VO_2 becomes dark in the metallic phase (**Figure 2**a). Raman spectra show that all the Raman features of monoclinic VO_2 diminish and disappear at temperatures above 80 °C, confirming the insulator-to-metal phase transition (Figure S3, Supporting Information). The transition appears gradual over a wide range of temperature for VO_2 thin films, due to its poly-crystalline nature (grain size ≈ 100 nm) and the substrate clamping strain, which leads to transitions at different temperatures in different grains (65 °C–85 °C, Figure 2a).[25,34,36]
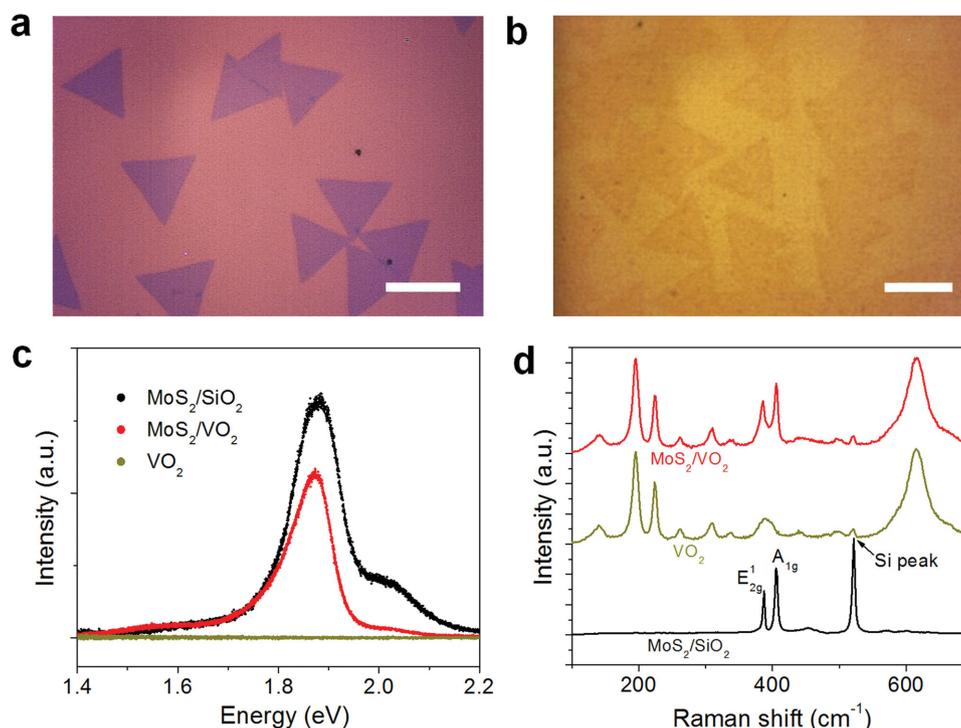
Figure 1. CVD monolayer MoS$_2$ transferred onto a) a SiO$_2$/Si substrate and b) a VO$_2$ thin film. c) PL spectra and d) Raman spectra of the monolayer MoS$_2$ on different substrates are shown. The thicknesses of VO$_2$ and SiO$_2$ are 150 nm and 300 nm, respectively. Scale bars, 10 μm.

The PL intensity of MoS$_2$ monolayers on VO$_2$ is found to increase monotonically with increasing temperature (Figure 2b). For comparison, we investigated two scenarios: MoS$_2$/VO$_2$ and MoS$_2$/SiO$_2$, and normalized their integrated PL intensities at variable temperatures with their respective values at room temperature. As shown in Figure 2c, the PL intensity of MoS$_2$/SiO$_2$ increases linearly and slightly by ≈50% over the temperature range from room temperature

to 100 °C. This increase is opposite to the behavior of conventional semiconductors and that of exfoliated monolayer MoS$_2$, and may be attributed to physi-sorption and desorption of O$_2$ or H$_2$O molecules when cooling and heating the CVD-grown MoS$_2$ in air, which is known to influence the PL of 2D semiconductors.[37] On the other hand, the PL intensity of MoS$_2$/VO$_2$ is enhanced by 400%–500% in the same temperature range. The enhancements are particularly
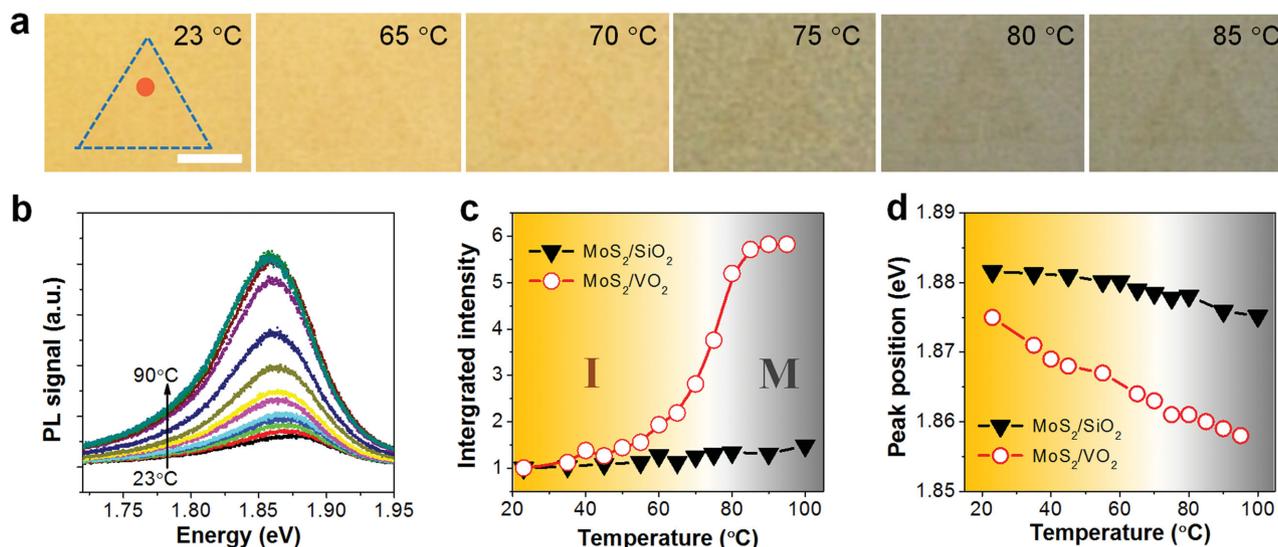
Figure 2. PL of monolayer MoS$_2$ across the MIT of VO$_2$. a) MoS$_2$/VO$_2$ at selected temperatures. The dashed triangle highlights the outline of a CVD-grown MoS$_2$ monolayer and the red dot indicates the position of the excitation laser spot for PL. Scale bar, 5 μm. b) PL spectra of MoS$_2$/VO$_2$ at various temperatures. c) Integrated PL intensity of MoS$_2$ on different substrates as a function of temperature. d) PL peak positions of MoS$_2$ on different substrates.

substantial during the MIT of VO_2, by ≈160% within only ≈20 °C for the MoS_2/VO_2 thin film (Figure 2c). In addition to the enhancement of PL intensity, the PL peak position also shifts. The peak position of MoS_2/SiO_2 slightly red-shifts with a slope of -8.9×10^{-5} eV per °C. This rate is almost tripled to -2.3×10^{-4} eV per °C for the MoS_2/VO_2 thin film, showing a high sensitivity of PL peak energy to temperature in the MoS_2/VO_2 system (Figure 2d).

3. Discussion

We focus our discussion on the large enhancement in the MoS_2 PL intensity across the MIT of VO_2, as this is the most prominent phenomenon. Several possible mechanisms could induce the PL enhancement, including strain (mechanical), charge or energy transfer (electronic), dielectric screening (dielectric), and optical interference (optical). In poly-crystal VO_2 thin films grown on SiO_2/Si, the films are generally textured and the c axis of the VO_2 rutile (metallic) phase, c_R, is orientated in plane, generating a small, isotropic, and compressive in-plane strain of ≈0.3% in average across the insulator to metal transition.[36] Effects of strain on the PL of monolayer MoS_2 have been previously quantified, and it was estimated to cause a shift in PL peak of ≈45 meV per %strain,[15] thus possibly leading to a PL peak shift of ≈13 meV across the MIT of VO_2. However, no turning points are observed in the curve of PL peak position versus temperature across the MIT temperature range (Figure 2d), implying a negligible strain contributed from the MIT of VO_2. This may be explained by the loose contact between MoS_2 and VO_2 as the surface of the polycrystalline VO_2 thin film is rough (5–10 nm, Figure S2, Supporting Information). On the other hand, even if MoS_2 was compressed by the MIT of VO_2 to ≈0.3%, its PL intensity would increase by only ≈10%,[15] which is much smaller than the observed PL enhancement. Therefore, the large enhancement in PL intensity cannot be primarily attributed to the VO_2-imposed strain.

Charge transfer may also occur between MoS_2 and VO_2, as they have a type-I band alignment (see Figure S4, Supporting Information). When insulating VO_2 interfaces with MoS_2, free electrons would transfer from MoS_2 to VO_2 due to the work function mismatch unless the diffusion electron flux (from MoS_2 to VO_2) balances with the drift electron flux (from VO_2 to MoS_2 by the built-in electric field). When the insulating VO_2 switches to the metallic phase, the work function of VO_2 increases and its Fermi level drops down by 0.1–0.2 eV, such that more electrons will transfer from MoS_2 to the metallic VO_2 until a new balance is established. It is well known that the PL intensity of monolayer MoS_2 can be enhanced if its optical transition switches from trion (i.e., two electrons and one hole) recombination to exciton (i.e., an electron–hole pair) recombination, which occurs when the free electron density in MoS_2 is depleted with electrostatic gating or doping.[10] This process should also be accompanied with a reduction in the spectral weight ratio of trions to excitons and a blue shift of the PL peak position, as the trion PL is ≈40 meV lower in energy than the exciton PL.[10] In our experiments, however, across the MIT of VO_2 we observed nearly no change in the peak ratio of excitons to trions of the MoS_2/VO_2 film (**Figure 3**a,b). It suggests that charge transfer may exist but is not the dominant mechanism for the effects. In addition, the monolayer MoS_2 does not affect the phase transition of VO_2, because the electron density required to trigger the phase transition of VO_2 is ultrahigh (≈10^{19} cm^{-3}),[38,39] which cannot be reached by the small amount, if any, of charge transferred between monolayer MoS_2 and bulk VO_2.

Energy transfer from MoS_2 to VO_2 through the dipole-dipole coupling, as described by the Förster theory,[40] may also occur because the band gap of MoS_2 is larger than VO_2 and the distance between them is in nanometer scale. Energy transfer efficiency would change during the MIT of VO_2 and affect the PL of MoS_2. However, VO_2 is either a heavily doped semiconductor (in I phase) or metal (in M phase), and thus its high density of free electrons could attenuate the dipole-dipole coupling to much extent, implying a weak energy transfer in MoS_2/VO_2 system.

Dielectric screening may also play a role in the change of the MoS_2 PL, because the dielectric properties of VO_2 vary
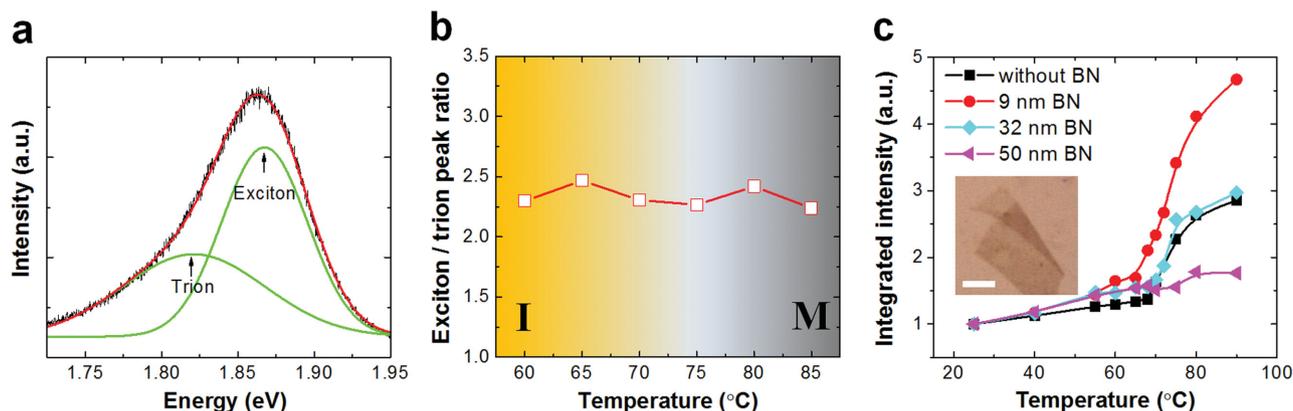
Figure 3. Optical properties in multilayer configurations. a) Double-peak fitting of a typical PL spectrum of $MoS_2/VO_2/SiO_2/Si$ at 60 °C, generating a trion peak (lower energy ≈ 1.82 eV) and an exciton peak (higher energy ≈ 1.86 eV). b) Spectral peak ratio of excitons to trions for $MoS_2/VO_2/SiO_2/Si$ across the phase transition of VO_2. The phase transition occurs in the range of 65 °C–85 °C for the VO_2 film. c) Experimental measurements of PL intensities in $MoS_2/BN/VO_2/SiO_2/Si$ multilayers with different BN thicknesses. The inset shows a BN flake, which is supported by VO_2 (background) and covered by a monolayer MoS_2 (invisible), with areas of three different thicknesses of BN; scale bar, 5 μm.

significantly across the MIT. In the visible spectral range relevant to this work, the imaginary part of the dielectric constant of VO₂ almost stays unchanged across the MIT, whereas the real part decreases when VO₂ switches from the insulating to metal phase.[41] This change would also alter the binding energy of excitons and trions in the proximate MoS₂ as well as their PL intensities. However, the nearly constant spectral ratio of excitons to trions of MoS₂ across the MIT of VO₂ (Figure 3b) suggests that the dielectric screening effect cannot be the primary mechanism responsible for the dramatic enhancement in the PL intensity of MoS₂.

One argument is that the change of roughness during the phase transition of VO₂ may also affect the PL of MoS₂. VO₂ undergoes a structural change with a strain no more than 1% along the a, b, or c axis of the rutile phase. For a VO₂ thin film used in our work with a thickness of 150 nm, therefore, the phase transition will introduce a change of surface roughness no more than 1.5 nm. If considering the poly-crystalline feature of VO₂ with a random distribution of crystal directions, the change would be even less than this value. It is much smaller than the original surface roughness (5–10 nm), and therefore it would not affect the contact between MoS₂ and VO₂ as well as the PL of MoS₂.

The dependence of Raman modes E_{2g}^1 and A_{1g} of MoS₂/VO₂ on temperatures is shown in Figure S1b in the Supporting Information. With increasing temperature, both E_{2g}^1 and A_{1g} modes of MoS₂ are softened and generally follow a linearly decreasing relationship. No deviation from the linear relationship are observed in the temperature-dependent curve of either E_{2g}^1 or A_{1g} mode across the MIT temperature range (65 °C–80 °C), further validating negligible strain or charge transfer effect imposed by the MIT of VO₂, because the MoS₂ E_{2g}^1 mode is sensitive to the strain while its A_{1g} mode is related to the doping level as we discussed before.

To further elucidate the mechanism of the PL enhancement, we introduced multilayer boron nitride (h-BN) between the MoS₂ and VO₂, forming a MoS₂/BN/VO₂/SiO₂/Si configuration. The thickness of the BN layers varies from 9 to 50 nm (Figure 3c), or 25 to 150 layers. With such a thick BN insertion, any possible charge transfer/tunneling or strain transmission between the MoS₂ and VO₂ will be fully blocked because of the large band gap (≈5.2 eV) and weak interlayer coupling within BN and at the MoS₂/BN/VO₂ interfaces. The energy transfer from MoS₂ to VO₂ will also be much weakened because the efficiency of the energy transfer is inversely proportional to the sixth power of the distance between MoS₂ and VO₂. The BN layer is also much thicker than the Bohr radius of excitons (≈3 nm) in monolayer MoS₂, which dielectrically isolates the MoS₂ monolayer from the VO₂. Therefore, if the PL enhancement is caused by any of the following mechanisms: charge or energy transfer, strain imposition, or dielectric screening, it should disappear in the MoS₂/BN/VO₂/SiO₂/Si system across the MIT of VO₂. However, as shown in Figure 3c, the PL intensity still shows a large enhancement across the MIT of VO₂, especially at a small thickness of BN layer (e.g., 9 nm). The magnitude of PL enhancement decreases when the BN thickness increases from 9 to 52 nm. This suggests that the PL enhancement still exists, but strongly depends on the thickness of the inserted BN layer. Therefore, we attribute the enhancement to optical interference effects.

Optical interference is a key factor that controls absorption and emission of atomically thin materials on a substrate. First, the incident light (488 nm) will transmit through the monolayer MoS₂ and the multilayers underneath, reflecting and refracting multiple times at the interfaces. The incident and outgoing waves interfere in the monolayer, generating an enhanced or weakened local E-field (E_a), which directly determines the absorbed light energy (A) of the monolayer MoS₂ following $A \propto |E_a|^2$ (**Figure 4**a). Secondly, the emitted PL (670 nm) from the MoS₂ going upward and downward follows similar traces as well (Figure 4b), yielding an E-field (E_e) at the far-field detector position, which defines the measured PL intensity $P \propto |E_e|^2$. The optical interference effect depends on dielectric properties and thicknesses of the monolayer MoS₂, the BN, the VO₂ layer, and the substrate.[23] The MoS₂ PL enhancement factor (β) across the MIT of VO₂ can thus be determined by

$$\beta = \frac{\left|E_a^M(488 \text{ nm}) \cdot E_e^M(670 \text{ nm})\right|^2}{\left|E_a^I(488 \text{ nm}) \cdot E_e^I(670 \text{ nm})\right|^2},$$

where the superscripts "M" and "I" indicate the case when the VO₂ is in the metallic phase and the insulating phase, respectively.

To investigate the effect of optical interference, we measured the reflectance of the VO₂ (150 nm)/SiO₂ (300 nm)/Si substrate at various temperatures. As shown in Figure S5 (Supporting Information), the reflectance clearly shows interference patterns in the spectra, and generally decreases in the range of visible light when the VO₂ turns from the insulating phase to the metallic phase. Note that when the MIT occurs, the reflectance is almost the same at the wavelength 488 nm while it changes much at the wavelength 670 nm. As the local electric field near the surface of VO₂ is determined by the interference between the incident light and the reflected light, it implies that the absorption of a monolayer MoS₂ on top of VO₂ at 488 nm should be not much different and the emission at 670 nm will be altered drastically across the MIT of VO₂. To quantitatively compare the PL before and after the VO₂ phase transition, numerical simulations were performed using a commercial finite element analysis software (COMSOL Multiphysics: wave optics module). Figure 4c,d reveal the E-field distribution at 488 nm (absorption) and 670 nm (emission) on insulating and metallic VO₂, respectively, under the condition of our experiments (thicknesses of VO₂ and SiO₂ are 150 nm and 300 nm, respectively). It shows that the absorption remains almost the same (Figure 4c), but the emission is greatly enhanced across the MIT of VO₂ (Figure 4d), revealing that the PL enhancement originates mostly from the interfered emission waves in our experimental configuration, which is consistent with the results revealed by the reflection spectra (Figure S5, Supporting Information). A simulation of the configuration with the insertion of a 9 nm thick BN layer shows similar results compared with the configuration without BN (see Figure S6, Supporting Information).
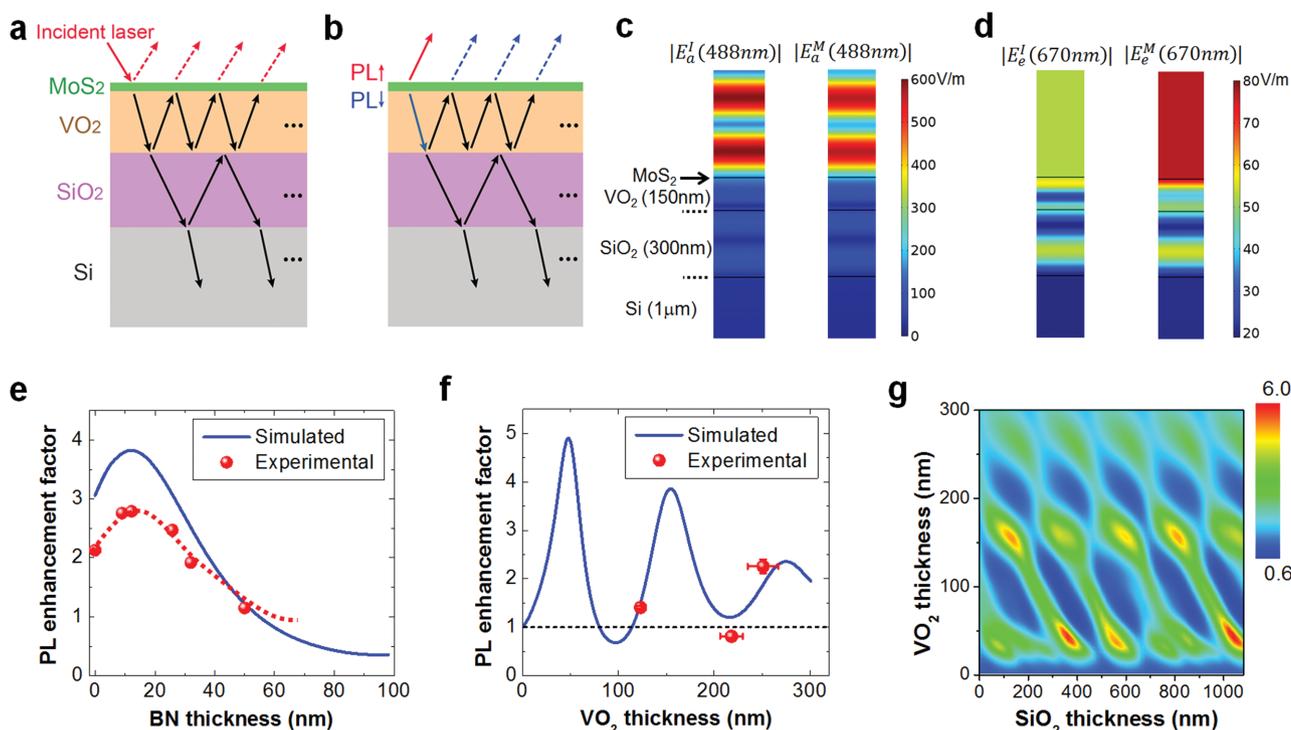
Figure 4. Optical interference effect. Illustrations of multi-step reflections and refractions in MoS₂/VO₂/SiO₂/Si multilayers, for a) the incident excitation light and b) the PL light. c) Distribution of E-field strength for the incident 488 nm laser light when the VO₂ is insulating (left) or metallic (right). d) Distribution of E-field strength for the PL light at 670 nm when VO₂ is insulating (left) or metallic (right). e) Dependence of PL enhancement factor on BN thickness when a BN layer is inserted between MoS₂ and VO₂ (150 nm) on a SiO₂ (300 nm)/Si substrate. The red dashed line guides for eyes. f) Dependence of PL enhancement factors on VO₂ thicknesses in a MoS₂/VO₂/SiO₂ (1 μm)/Si configuration. The black dashed line labels the factor value without PL enhancement or weakening. g) Contour of PL enhancement factors depending on both VO₂ and SiO₂ thicknesses.

Experimentally we define the enhancement factor, β, as the ratio of the integrated intensity of the MoS₂ PL immediately after to immediately before the phase transition of VO₂. This corresponds to the PL intensities with the metallic phase (90 °C) and that with the insulating phase (65 °C) for the VO₂ film used in the BN insertion experiment (Figure 3c). Figure 4e shows the simulated enhancement factor for various BN thicknesses. The simulated factor initially increases and peaks at the BN thickness of ≈12 nm, and then decreases with the increase of the BN thickness. The experimental β is constantly lower than the simulated values, but follows the non-monotonic trend of the theoretical dependence (Figure 4e), validating the interference effect as the dominant mechanism of the PL enhancement. The systematically lower experimental value of β may result from inaccurate dielectric constants of VO₂ and BN used in the simulation, or possible vacuum or air gaps existing between the MoS₂, BN, and VO₂.

This simple, interference-enabled PL enhancement provides an effective, reversible way to modulate the PL intensity of monolayer MoS₂. The PL enhancement factor can be further increased by optimizing the thickness of VO₂ and SiO₂. The enhancement factor is simulated and measured as a function of the VO₂ or SiO₂ thicknesses. Figure 4f reveals an interference feature that the PL enhancement factor oscillates with variation in the VO₂ thickness in a MoS₂/VO₂/SiO₂/Si configuration. The experimental data show quite different β values but all of the data points generally

sit on the simulated curve, which further validates that the PL enhancement originates from the interference effect. Figure 4g shows a simulated contour of β values depending on both VO₂ and SiO₂ thicknesses with periodic patterns in two dimensions. In our simulation range, the maxima of the PL enhancement factor is ≈6.0, occurring at 41 nm thick VO₂ and 1.04 μm thick SiO₂. Increasing the VO₂ thickness beyond 250 nm results in a weaker dependence of β on SiO₂ thickness, because at such thicknesses, the light absorption of VO₂ becomes strong[33] and the interference occurs mostly between the incident beam and the beam reflected by the VO₂ surface. Similar simulation with a BN layer is plotted in Figure S6 (Supporting Information). In the case of thick VO₂, β tends to saturate at ≈2, which is consistent with our experimental value for MoS₂ on a 1 μm thick VO₂ microplate (Figure S7, Supporting Information). Figure 4g also shows that in many cases, the enhancement factor is smaller than 1, predicting a reduction of the PL intensity of MoS₂ across the MIT of VO₂, which is also observed in our experimental data (Figure 4f).

As the VO₂ poly-crystal thin films usually exhibit a wide hysteresis in its MIT between the heating and cooling process,[36] a non-volatile memory effect can be realized, in which arbitrary patterns of the metallic phase can be laser written on an insulating VO₂ film. As shown in **Figure 5**a, when the VO₂ film is globally heated to the middle temperature T_{MIT} (≈68 °C), the film is still in the insulating phase; then
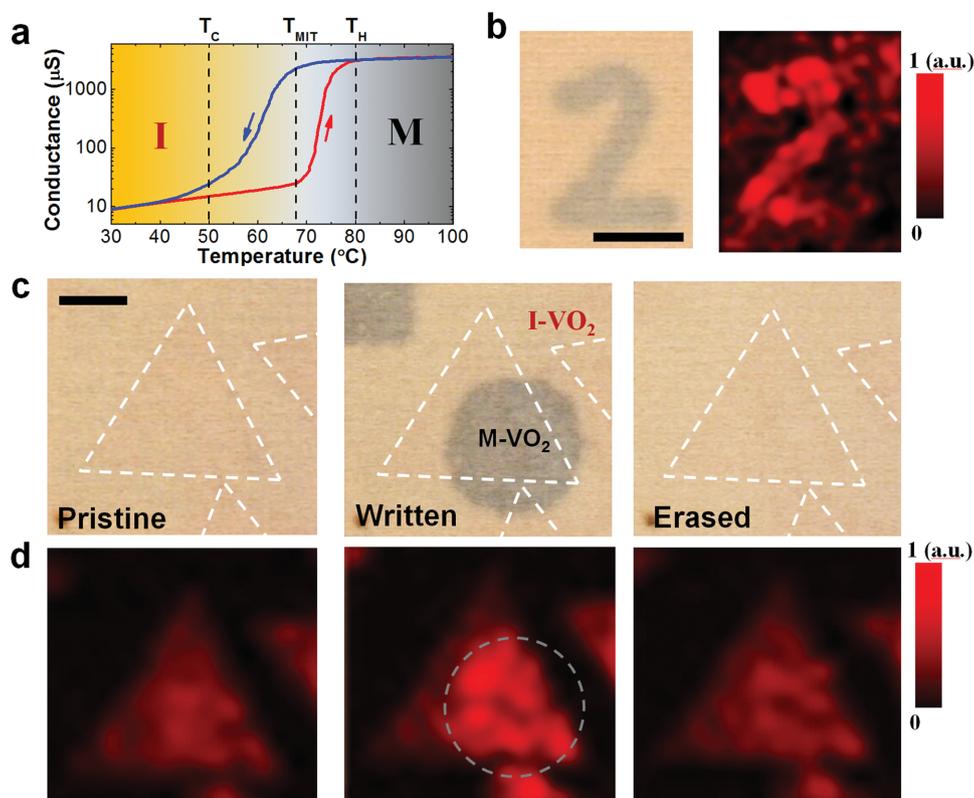
Figure 5. Writing and erasing desired patterns of MoS$_2$ PL. a) Temperature dependence of electrical conductance of a typical VO$_2$ film, showing a hysteresis of the MIT between heating and cooling processes. b) Laser-writing metallic regions with shape of a "2" on a MoS$_2$ monolayer covered insulating VO$_2$ film, translating to an identical MoS$_2$ PL pattern. Note that a continuous MoS$_2$ monolayer covers the entire area of image. The substrate is maintained globally at 68 °C. Laser-writing c) a metallic VO$_2$ circle, which overlaps with a MoS$_2$ monolayer triangle, and enhances its PL intensity within d) the overlapped area; the pattern is erased by global cooling to ≈50 °C. Scale bars, 5 μm.

a focused laser (488 nm, ≈80 μW) is used to locally heat the VO$_2$ to T_H, writing an arbitrary metallic pattern in the insulating VO$_2$. This metallic pattern would stay even when the writing laser is turned off, unless the global temperature is cooled to T_C, which completely erases the pattern. Following the PL modulation of MoS$_2$ by the MIT in VO$_2$, the metallic pattern in VO$_2$ would translate to an identical pattern in the PL map of the overlaid MoS$_2$. Figure 5b shows a "2"-shaped domain of metallic VO$_2$ that has been written by the laser. It locally enhances the PL intensity of the overlaid MoS$_2$ monolayer, leading to the same pattern in the PL mapping image. Figure 5c,d show that a circular region of metallic VO$_2$ partially overlaps with a triangle of monolayer MoS$_2$, enhancing the PL of MoS$_2$ within the overlapped area. Due to the reversibility of the MIT, simply cooling the system to ≈50 °C can reset the metallic VO$_2$ back to the insulating phase (Figure 5c), such that the PL image is erased (Figure 5d), and a new, different pattern can be written in the same area. These writing and erasing processes can be repeated many times on the MoS$_2$/VO$_2$ structure without degradation of the image quality. A contactless, nonvolatile, rewritable, and spatially selective modulation of MoS$_2$ PL is thus demonstrated. Further, some techniques can lower the phase transition temperature of VO$_2$, such as with tungsten doping,[42] so that only a small amount of energy would be required to trigger the phase transition of doped VO$_2$ and modulate the PL of MoS$_2$.

It will provide a more efficient modulation method with much lower energy consumption.

4. Conclusions

In summary, by interfacing a MoS$_2$ monolayer with a VO$_2$ film undergoing a metal–insulator phase transition, we demonstrate a versatile way to modulate the PL intensity of monolayer MoS$_2$ with rewritability, spatial selectivity, and large ON/OFF ratio. The existence of similar PL modulation with an insertion of insulating boron nitride (h-BN) layers between MoS$_2$ and VO$_2$, as well as the almost unchanged spectral weight ratios of trions to excitons of MoS$_2$ across the MIT of VO$_2$, excludes strain, charge transfer, or dielectric screening effect as the dominant mechanism. As a result, optical interference effect is found to be the primary mechanism responsible for the modulation. Simulation shows that the PL of MoS$_2$ can be drastically strengthened or weakened across the MIT of VO$_2$ depending on the thickness of each layer in the structure. The drastic modulation of PL in monolayer semiconductors may enable new applications in novel sensors, displays and switches. The development of these devices leave many interesting topics for future work, which would further deepen the understanding of the mechanism for the modulation by such active substrates, as well as the

possible interface interaction between 2D semiconductors and functional oxides.

5. Experimental Section

Fabrications: Poly-crystalline VO$_2$ thin films and single-crystal VO$_2$ microplates were prepared by pulsed laser deposition (PLD) and physical vapor deposition (PVD), respectively, on Si substrates with thermal SiO$_2$ (SiO$_2$/Si). The details of syntheses were described in our previous work.[36,43–45] Monolayer MoS$_2$ samples were synthesized by chemical-vapor deposition (CVD) on SiO$_2$/Si substrates using MoO$_3$ and S powders as precursors, which was also described in our previous work.[22,46] Boron nitride (BN) flakes were mechanically exfoliated from a bulk *h*-BN crystal onto SiO$_2$/Si substrates. The thicknesses of VO$_2$ thin films, VO$_2$ microplates, and BN flakes were determined by an atomic force microscope (AFM, Bruker Multimode). To stack MoS$_2$/VO$_2$/SiO$_2$/Si structures, as-grown MoS$_2$ was spin-coated with 200 nm thick PMMA, released out of the substrate by etching with 1 M KOH solution for 1–2 h, and transferred onto VO$_2$-coated SiO$_2$/Si substrates. The PMMA was then dissolved by acetone, leaving monolayer MoS$_2$ stacked onto the VO$_2$. To stack MoS$_2$/BN/VO$_2$/SiO$_2$/Si structures, exfoliated BN flakes and as-grown MoS$_2$ films were transferred in sequence onto VO$_2$-coated SiO$_2$/Si substrates by using the same PMMA-assisted transfer process.

Measurements: Raman and PL measurements were performed using a Renishaw Invia instrument with an excitation laser wavelength of 488 nm. Spectra were collected by a 100× objective lens; the focused laser spot was ≈1.5 µm in diameter, and the laser power was set at a low value of ≈20 µW to avoid over-heating effects. For the laser writing process, VO$_2$ substrates were globally heated to 65 °C. The laser was then set to a higher power of ≈80 µW passing through the same lens, which further heats up the VO$_2$ film by an estimated temperature rise of ≈10 °C and locally induces the MIT of VO$_2$.

Simulations: In COMSOL simulations, a 2D air/MoS$_2$/BN/VO$_2$/SiO$_2$/Si multilayer model with periodic boundary conditions was built to simulate uniform illumination over the entire multilayer structure. Thicknesses of all layers were varied during the simulation. A single simulation consists of two steps. In the first step, a plane wave with 488 nm wavelength was launched from the top to imitate the PL excitation laser. Power loss in the MoS$_2$ layer was recorded. We assumed that all power absorbed by the MoS$_2$ layer contributed to its illumination. In the second step, we set the MoS$_2$ layer as a light source, and determined how much power was detectable by a detector at far field. Light of 670 nm was generated by passing an oscillating electric current in the MoS$_2$ layer. The same current density was used for all simulations. We then recorded power flow from the MoS$_2$ layer to the air, which imitated detectable power by a detector at far field. We used the product of the power loss in step 1 and the power flow in step 2 to define relative PL power in arbitrary units. Using such two-step simulations, we could get the relative PL power for all desired layer thicknesses and temperature combinations. Here, we used refractive indexes of MoS$_2$, BN and dielectric constants of VO$_2$ at 30 °C (insulating) and 85 °C (metallic) in literature[41,47,48] as the values in our simulation.

Supporting Information

Supporting Information is available from the Wiley Online Library or from the author.

Acknowledgements

[1] B. Radisavljevic, A. Radenovic, J. Brivio, V. Giacometti, A. Kis, *Nat. Nanotechnol.* **2011**, *6*, 147.
[2] A. K. Geim, I. V. Grigorieva, *Nature* **2013**, *499*, 419.
[3] K. F. Mak, C. Lee, J. Hone, J. Shan, T. F. Heinz, *Phys. Rev. Lett.* **2010**, *105*, 136805.
[4] A. Splendiani, L. Sun, Y. Zhang, T. Li, J. Kim, C. Y. Chim, G. Galli, F. Wang, *Nano Lett.* **2010**, *10*, 1271.
[5] O. Lopez-Sanchez, D. Lembke, M. Kayci, A. Radenovic, A. Kis, *Nat. Nanotechnol.* **2013**, *8*, 497.
[6] W. J. Yu, Y. Liu, H. L. Zhou, A. X. Yin, Z. Li, Y. Huang, X. F. Duan, *Nat. Nanotechnol.* **2013**, *8*, 952.
[7] Q. H. Wang, K. Kalantar-Zadeh, A. Kis, J. N. Coleman, M. S. Strano, *Nat. Nanotechnol.* **2012**, *7*, 699.
[8] H. T. Yuan, X. Q. Wang, B. Lian, H. J. Zhang, X. F. Fang, B. Shen, G. Xu, Y. Xu, S. C. Zhang, H. Y. Hwang, Y. Cui, *Nat. Nanotechnol.* **2014**, *9*, 851.
[9] X. Zhou, J. X. Cheng, Y. B. Zhou, T. Cao, H. Hong, Z. M. Liao, S. W. Wu, H. L. Peng, K. H. Liu, D. P. Yu, *J. Am. Chem. Soc.* **2015**, *137*, 7994.
[10] K. F. Mak, K. L. He, C. Lee, G. H. Lee, J. Hone, T. F. Heinz, J. Shan, *Nat. Mater.* **2013**, *12*, 207.
[11] Z. Li, S.-W. Chang, C.-C. Chen, S. B. Cronin, *Nano Res.* **2014**, *7*, 973.
[12] S. Tongay, J. Zhou, C. Ataca, J. Liu, J. S. Kang, T. S. Matthews, L. You, J. B. Li, J. C. Grossman, J. Q. Wu, *Nano Lett.* **2013**, *13*, 2831.
[13] S. Mouri, Y. Miyauchi, K. Matsuda, *Nano Lett.* **2013**, *13*, 5944.
[14] Y. C. Wang, J. Z. Ou, S. Balendhran, A. F. Chrimes, M. Mortazavi, D. D. Yao, M. R. Field, K. Latham, V. Bansal, J. R. Friend, S. Zhuiykov, N. V. Medhekar, M. S. Strano, K. Kalantar-Zadeh, *ACS Nano* **2013**, *7*, 10083.
[15] H. J. Conley, B. Wang, J. I. Ziegler, R. F. Haglund, S. T. Pantelides, K. I. Bolotin, *Nano Lett.* **2013**, *13*, 3626.
[16] S. B. Desai, G. Seol, J. S. Kang, H. Fang, C. Battaglia, R. Kapadia, J. W. Ager, J. Guo, A. Javey, *Nano Lett.* **2014**, *14*, 4592.
[17] Z. L. Ye, T. Cao, K. O'Brien, H. Y. Zhu, X. B. Yin, Y. Wang, S. G. Louie, X. Zhang, *Nature* **2014**, *513*, 214.

[18] M. Buscema, G. A. Steele, H. S. J. van der Zant, A. Castellanos-Gomez, *Nano Res.* **2014**, *7*, 561.

[19] Y. Li, Z. Qi, M. Liu, Y. Wang, X. Cheng, G. Zhang, L. Sheng, *Nanoscale* **2014**, *6*, 15248.

[20] D. Sercombe, S. Schwarz, O. Del Pozo-Zamudio, F. Liu, B. J. Robinson, E. A. Chekhovich, I. I. Tartakovskii, O. Kolosov, A. I. Tartakovskii, *Sci. Rep.* **2013**, *3*, 3489.

[21] Y. Lin, X. Ling, L. Yu, S. Huang, A. L. Hsu, Y. H. Lee, J. Kong, M. S. Dresselhaus, T. Palacios, *Nano Lett.* **2014**, *14*, 5569.

[22] K. Liu, Q. M. Yan, M. Chen, W. Fan, Y. H. Sun, J. Suh, D. Y. Fu, S. Lee, J. Zhou, S. Tongay, J. Ji, J. B. Neaton, J. Q. Wu, *Nano Lett.* **2014**, *14*, 5097.

[23] Y. Y. Wang, Z. H. Ni, Z. X. Shen, H. M. Wang, Y. H. Wu, *Appl. Phys. Lett.* **2008**, *92*, 043121.

[24] S. L. Li, H. Miyazaki, H. Song, H. Kuramochi, S. Nakaharai, K. Tsukagoshi, *ACS Nano* **2012**, *6*, 7381.

[25] J. Cao, E. Ertekin, V. Srinivasan, W. Fan, S. Huang, H. Zheng, J. W. L. Yim, D. R. Khanal, D. F. Ogletree, J. C. Grossmanan, J. Wu, *Nat. Nanotechnol.* **2009**, *4*, 732.

[26] C. Xiang-Bai, *J. Korean Phys. Soc.* **2011**, *58*, 100.

[27] C. Cheng, K. Liu, B. Xiang, J. Suh, J. Q. Wu, *Appl. Phys. Lett.* **2012**, *100*, 4.

[28] C. Lee, H. Yan, L. E. Brus, T. F. Heinz, J. Hone, S. Ryu, *ACS Nano* **2010**, *4*, 2695.

[29] H. Li, Q. Zhang, C. C. R. Yap, B. K. Tay, T. H. T. Edwin, A. Olivier, D. Baillargeat, *Adv. Funct. Mater.* **2012**, *22*, 1385.

[30] B. Chakraborty, A. Bera, D. V. S. Muthu, S. Bhowmick, U. V. Waghmare, A. K. Sood, *Phys. Rev. B* **2012**, *85*, 4.

[31] M. Buscema, G. A. Steele, H. S. J. van der Zant, A. Castellanos-Gomez, *Nano Res.* **2014**, *7*, 561.

[32] C. Rice, R. J. Young, R. Zan, U. Bangert, D. Wolverson, T. Georgiou, R. Jalil, K. S. Novoselov, *Phys. Rev. B* **2013**, *87*, 5.

[33] D. Y. Fu, K. Liu, T. Tao, K. Lo, C. Cheng, B. Liu, R. Zhang, H. A. Bechtel, J. Q. Wu, *J. Appl. Phys.* **2013**, *113*, 043707.

[34] J. Q. Wu, Q. Gu, B. S. Guiton, N. P. de Leon, O. Y. Lian, H. Park, *Nano Lett.* **2006**, *6*, 2313.

[35] C. Ko, Z. Yang, S. Ramanathan, *ACS Appl. Mater. Interfaces* **2011**, *3*, 3396.

[36] K. Liu, C. Cheng, Z. T. Cheng, K. V. Wang, R. Ramesh, J. Q. Wu, *Nano Lett.* **2012**, *12*, 6302.

[37] S. Tongay, J. Zhou, C. Ataca, K. Lo, T. S. Matthews, J. Li, J. C. Grossman, J. Wu, *Nano Lett.* **2012**, *12*, 5576.

[38] J. Cao, W. Fan, K. Chen, N. Tamura, M. Kunz, V. Eyert, J. Wu, *Phys. Rev. B* **2010**, *82*, 4.

[39] K. Liu, D. Y. Fu, J. B. Cao, J. Suh, K. X. Wang, C. Cheng, D. F. Ogletree, H. Guo, S. Sengupta, A. Khan, C. W. Yeung, S. Salahuddin, M. M. Deshmukh, J. Q. Wu, *Nano Lett.* **2012**, *12*, 6272.

[40] T. Forster, *Ann. Phys.* **1948**, *2*, 55.

[41] J. B. Kana Kana, J. M. Ndjaka, G. Vignaud, A. Gibaud, M. Maaza, *Opt. Commun.* **2011**, *284*, 807.

[42] S. Lee, C. Cheng, H. Guo, K. Hippalgaonkar, K. Wang, J. Suh, K. Liu, J. Q. Wu, *J. Am. Chem. Soc.* **2013**, *135*, 4850.

[43] K. Liu, C. Cheng, J. Suh, R. Tang-Kong, D. Y. Fu, S. Lee, J. Zhou, L. O. Chua, J. Q. Wu, *Adv. Mater.* **2014**, *26*, 1746.

[44] K. Wang, C. Cheng, E. Cardona, J. Y. Guan, K. Liu, J. Q. Wu, *ACS Nano* **2013**, *7*, 2266.

[45] C. Cheng, H. Guo, A. Amini, K. Liu, D. Fu, J. Zou, H. S. Song, *Sci. Rep.* **2014**, *4*, 5.

[46] S. Tongay, W. Fan, J. Kang, J. Park, U. Koldemir, J. Suh, D. S. Narang, K. Liu, J. Ji, J. B. Li, R. Sinclair, J. Q. Wu, *Nano Lett.* **2014**, *14*, 3185.

[47] R. Geick, C. H. Perry, G. Rupprecht, *Phys. Rev.* **1966**, *146*, 543.

[48] H. Zhang, Y. G. Ma, Y. Wan, X. Rong, Z. Xie, W. Wang, L. Dai, *Sci. Rep.* **2015**, *5*, 7.

NANO MICRO
small

Supporting Information

Modulating Photoluminescence of Monolayer Molybdenum Disulfide by Metal–Insulator Phase Transition in Active Substrates

Jiwei Hou, Xi Wang, Deyi Fu, Changhyun Ko, Yabin Chen, Yufei Sun, Sangwook Lee, Kevin X. Wang, Kaichen Dong, Yinghui Sun, Sefaattin Tongay, Liying Jiao, Jie Yao, Kai Liu,* and Junqiao Wu*

Supporting Information

Modulating Photoluminescence of Monolayer Molybdenum Disulfide by Metal-Insulator Phase Transition in Active Substrates

Jiwei Hou,[#] Xi Wang,[#] Deyi Fu, Changhyun Ko, Yabin Chen, Yufei Sun, Sangwook Lee, Kevin X. Wang, Kaichen Dong, Yinghui Sun, Sefaattin Tongay, Liying Jiao, Jie Yao, Kai Liu,[*] Junqiao Wu[*]

1. Raman modes of MoS$_2$ on different substrates and at different temperatures
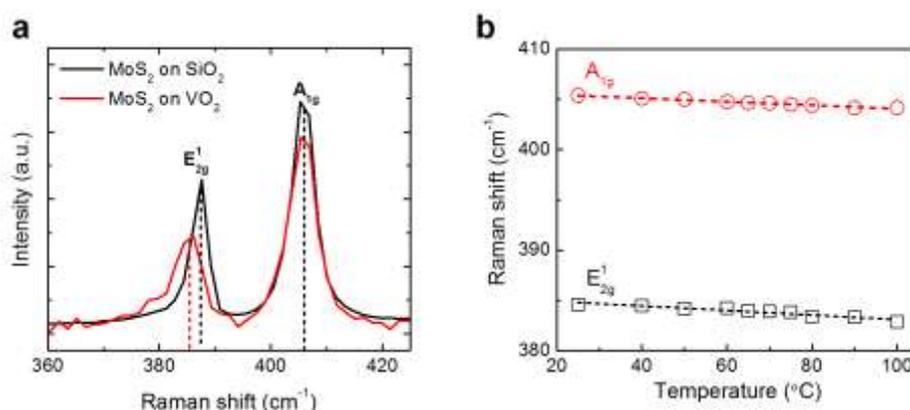
Figure S1. (a) Featured Raman modes of monolayer MoS$_2$ on SiO$_2$ and VO$_2$, respectively. The spectra are extracted from Figure 1d in the range of 360 ~ 425 cm^{-1}. The spectra of MoS$_2$ on VO$_2$ is obtained by subtracting the Raman spectrum of VO$_2$ from that of MoS$_2$/VO$_2$. (b) Dependence of MoS$_2$ E$_{2g}^1$ and A$_{1g}$ modes on temperature for MoS$_2$/VO$_2$.

2. Topology of as-deposited VO$_2$ thin film
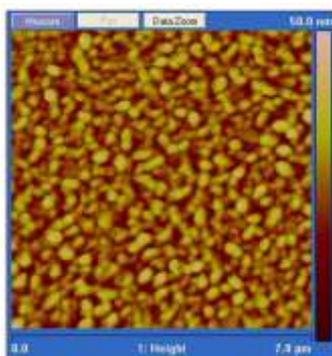
Figure S2. Atomic force microscopic (AFM) image of VO$_2$ thin film, showing a polycrystalline feature and rough surface.

3. Raman spectra of VO$_2$ at various temperatures
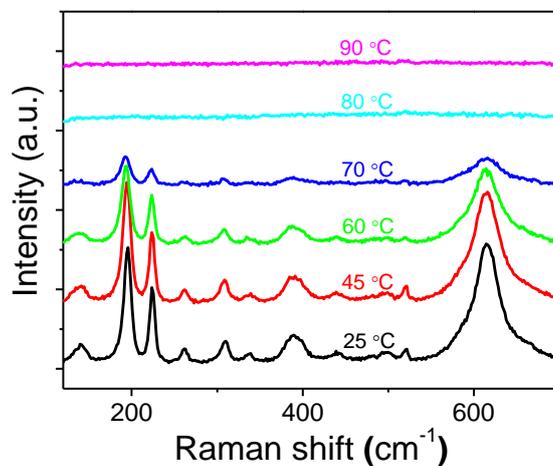
Figure S3. Raman spectra of a VO$_2$ film, suggesting a phase transition from monoclinic (insulator) phase to rutile (metal) phase during heating.

4. Band alignment of MoS$_2$ and VO$_2$
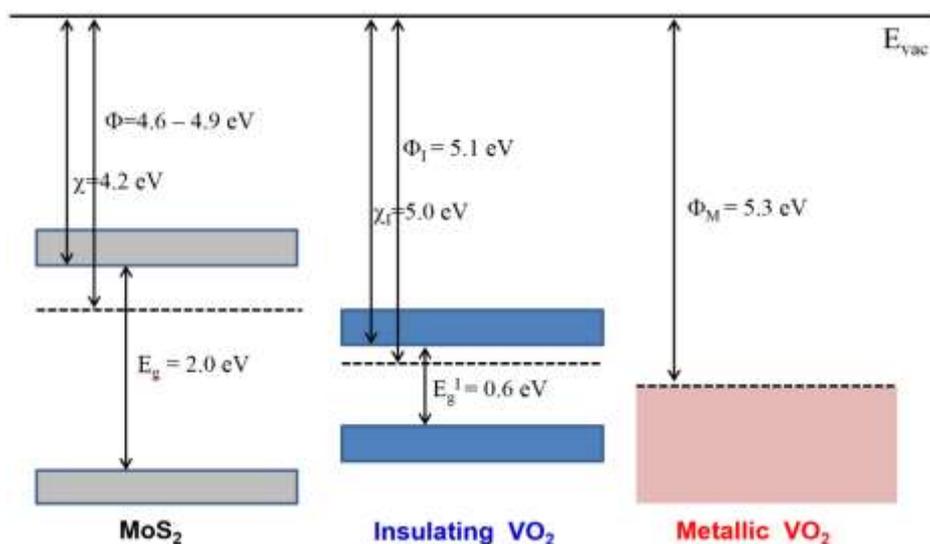
Figure S4. Band alignment of MoS$_2$, insulating VO$_2$ and metallic VO$_2$ obtained from references.[1-4]

5. Optical reflectance of a VO$_2$/SiO$_2$/Si substrate at various temperatures
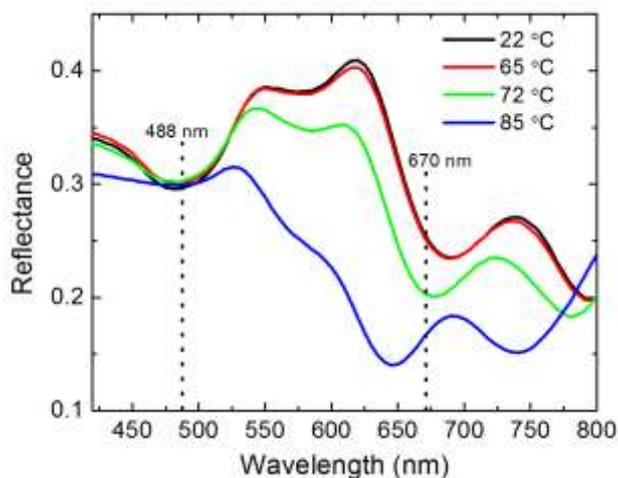
Figure S5. Dependence of the reflectance of VO$_2$ (150 nm)/SiO$_2$ (300 nm)/Si on incident light wavelengths at various temperatures.

6. Monolayer MoS$_2$ on BN/VO$_2$
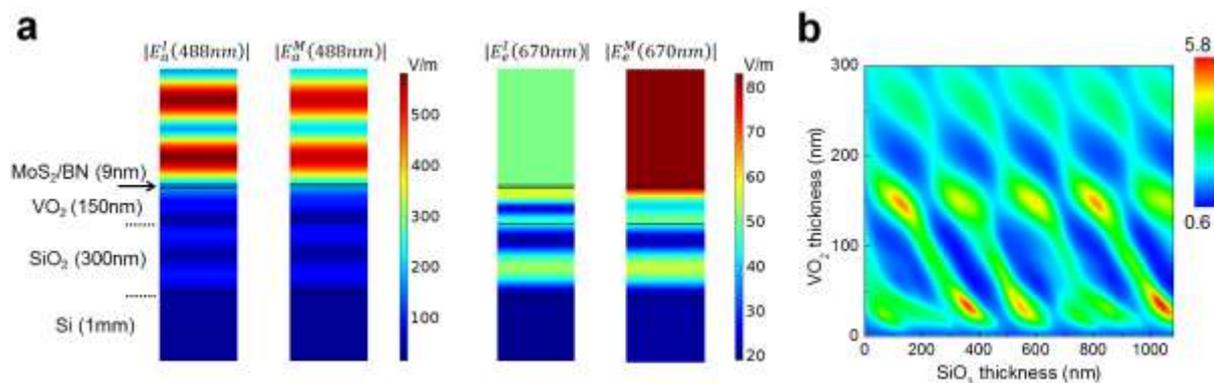
Figure S6. Simulated E-field and PL enhancement factors for the monolayer MoS$_2$/BN/VO$_2$/SiO$_2$/Si configuration, where the BN thickness is 9 nm. The simulated results show little difference compared with the simulation demonstrated in Figure 3d, 3e, and 3f, suggesting that the BN layer is too thin to dramatically affect the local E-field around the surface of VO$_2$.

7. Monolayer MoS$_2$ on VO$_2$ microplate
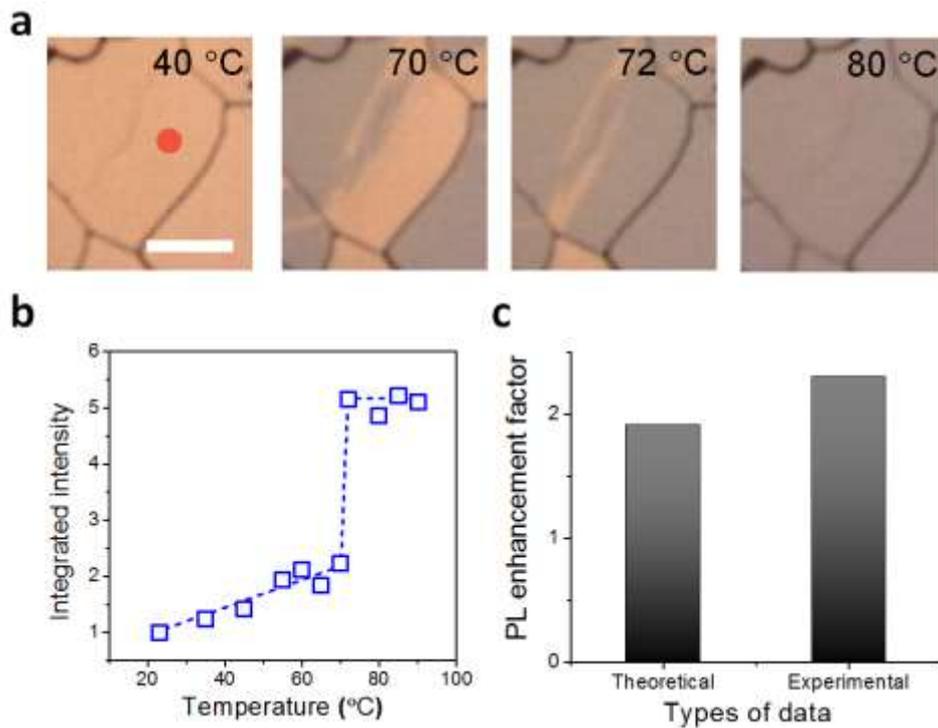
Figure S7. Monolayer MoS$_2$ on 1 μm-thick VO$_2$ microplates. Single-crystal micro-plates of VO$_2$ were prepared by physical vapor deposition (PVD).[5, 6] (a) MoS$_2$/VO$_2$-plate at selected temperatures. The microplates consist of single-crystal VO$_2$ grains with visible grain boundaries and show a very sharp phase transition. The entire view field is covered with a single MoS$_2$ monolayer. The laser spot for measurements are indicated by the solid red circle. The phase transition of VO$_2$ at the spot occurs abruptly from 70 to 72 °C. Scale bar, 5 μm. (b) Integrated PL intensity of MoS$_2$ on the VO$_2$ microplate as a function of temperature. (c) Comparison of experimental and theoretical PL enhancement factors across the phase transition of VO$_2$. The theoretical factor was calculated by the same method with the same dielectric parameters as described in the main text.

[1]   M. S. Choi, G. H. Lee, Y. J. Yu, D. Y. Lee, S. H. Lee, P. Kim, J. Hone, W. J. Yoo, *Nat Commun* 2013, *4*, 1624.
[2]   C. Miller, M. Triplett, J. Lammatao, J. Suh, D. Fu, J. Wu, D. Yu, *Phys. Rev. B* 2012, *85*.

[3]   K. Martens, I. P. Radu, S. Mertens, X. Shi, L. Nyns, S. Cosemans, P. Favia, H. Bender, T. Conard, M. Schaekers, S. De Gendt, V. Afanas'ev, J. A. Kittl, M. Heyns, M. Jurczak, *J. Appl. Phys.* 2012, *112*, 124501.

[4]   Y. Zhou, S. Ramanathan, *J. Appl. Phys.* 2013, *113*, 213703.

[5]   K. Wang, C. Cheng, E. Cardona, J. Y. Guan, K. Liu, J. Q. Wu, *ACS Nano* 2013, *7*, 2266.

[6]   C. Cheng, H. Guo, A. Amini, K. Liu, D. Fu, J. Zou, H. S. Song, *Sci. Rep.* 2014, *4*, 5.